

**A study of the response of deep tropical clouds to mesoscale processes:
Part II: Sensitivities to microphysics, radiation, and surface fluxes.**

Daniel Johnson, Wei-Kuo Tao, and Joanne Simpson
Submitted to: Journal of Atmospheric Sciences

Popular Summary

Interactions between deep convective clouds and the large-scale environment are key to understanding climate change. This is especially true for deep clouds over the warm tropical waters of the western Pacific and east Indian oceans, which produce large atmospheric heating rates, and greatly influence the general circulation of the atmosphere. Cloud systems interact with the environment through heat and moisture transfer with the surface (Ocean), radiative transfer processes, conversions of water between its three phases (vapor, liquid and ice, also known as microphysical processes), and the transport of heat and moisture through cloud-generated horizontal and vertical motions. These processes must be better understood before the accuracy of models used to predict climate change can be substantially improved. In this paper, a model (the Goddard Cumulus Ensemble Model; GCEM), which resolves clouds using a horizontal grid spacing of 1 km, is used to study the relative importance of cloud processes to the large-scale environment for an active convective period over the western tropical Pacific.

This study shows that when air-sea heat and moisture transfer is eliminated, the mean atmosphere is much cooler and drier, precipitation is less, and cloud coverage is much greater. Solar and infrared radiation is found to have only minimal effects on the overall mean temperature, humidity, cloudiness, and precipitation. However, radiation processes do play a significant role on the cloud temperature and structures above 12 km and on the overall mean vertical circulations. The removal of ice processes produces major changes in the structure of the cloud, and leads to narrow but intense bands of rainfall. The elimination of the melting of ice produces a much more solid water mass in the lower levels of the atmosphere, and a warmer and moister layer near the surface. These results are presented along with a detailed quantitative measure of the contributions from cloud microphysics, radiation, and air-sea fluxes on the overall mean temperature and moisture budgets for each case.

Abstract

The Goddard Cumulus Ensemble (GCE) model is used to examine the sensitivities of surface fluxes, explicit radiation, and ice microphysical processes on multi-day simulations of deep tropical convection over the Tropical Ocean Global Atmosphere Coupled Ocean-Atmosphere Response Experiment (TOGA COARE). The simulations incorporate large-scale advective temperature and moisture forcings, as well as large-scale momentum, that are updated every time step on a periodic lateral boundary grid.

This study shows that when surface fluxes are eliminated, the mean atmosphere is much cooler and drier, convection and CAPE are much weaker, precipitation is less, and cloud coverage in stratiform regions much greater. Surface fluxes using the TOGA COARE flux algorithm are weaker than with the aerodynamic formulation, but closer to the observed fluxes. In addition, similar trends noted above for the case without surface fluxes are produced for the TOGA flux case, albeit to a much lesser extent. The elimination of explicit shortwave and longwave radiation is found to have only minimal effects on the mean thermodynamics, convection, and precipitation. However explicit radiation does have a significant impact on cloud temperatures and structure above 200 mb and on the overall mean vertical circulation.

The removal of ice processes produces major changes in the structure of the cloud. Much of the liquid water is transported aloft and into anvils above the melting layer (600 mb),

leaving narrow, but intense bands of rainfall in convective regions. The elimination of melting processes leads to greater hydrometeor mass below the melting layer, and produces a much warmer and moister boundary layer, leading to a greater mean CAPE. Finally, the elimination of the graupel species has only a small impact on mean total precipitation, thermodynamics, and dynamics of the simulation, but does produce much greater snow mass just above the melting layer. Some of these results differ from previous CRM studies of tropical systems, which is likely due to the type of simulated system, total time integration, and model setup.

**A study of the response of deep tropical clouds to large-scale thermodynamic forcings.
Part II: Sensitivities to microphysics, radiation, and surface fluxes.**

D. E. Johnson^{1,2}, W.-K. Tao², and J. Simpson²

¹*Goddard Earth Sciences and Technology Center
University of Maryland, Baltimore County
Baltimore, MD*

²*Laboratory for Atmospheres
NASA/Goddard Space Flight Center
Greenbelt, MD 20771*

Journal of the Atmospheric Sciences
(March 16, 2004)

Corresponding author address: Dr. Daniel E. Johnson, Mesoscale Atmospheric Processes
Branch, Code 912, NASA/GSFC, Greenbelt, MD 20771
Email: djohnson@agnes.gsfc.nasa.gov

1. Introduction

Problems commonly confronted by general circulation models (GCMs) involve not only in determining how cloud systems affect the large-scale fields, but also how the evolution, maintenance, dissipation, and structure of cloud systems relate to large-scale variables (e.g., large-scale forcings, microphysics, radiative transfer, boundary layer turbulence, and surface fluxes). In part I (Johnson et al., 2002), we mentioned that the CRM can be used to quantify the cumulative large-scale effects of cloud systems and proceeded to examine the role of model setup (numerics and grid specification) in the development of deep convection. In this paper we will demonstrate how the CRM can be utilized to study the sensitivities of microphysical processes, radiative transfer, and air-sea interactions on the development, maintenance, and structure of cloud systems. A goal of this study is to improve the understanding of cloud processes for parameterizations GCMs by understanding the major physical processes involved in clouds. A number of field campaigns have been conducted over the years over tropical regions including GARP Atlantic Tropical Experiment (GATE; 1974), the Tropical Ocean/Global Atmosphere-Coupled Ocean/Atmospheric Response Experiment (TOGA-COARE; 1992), and the South China Sea Experiment (SCSMEX; 1998), which have and can be utilized by CRMs in modeling studies of deep tropical clouds and ensembles (e.g. Xu and Randall, 1998; Donner et al. 1999; Grabowski et al. 1999; Tao et al. 2004). As in part I, this study will involve Case 2 from the Global Energy and Water-Cycle Experiment (GEWEX) Cloud System Study (GCSS), Working Group 2 (WG2; deep

convective clouds), which is an 8-day simulation of deep tropical convection over the Intensive Flux Array (IFA) of the TOGA-COARE (Moncrieff et al. 1997).

The major objectives of this paper are to investigate the response and behavior of deep tropical cloud systems and precipitation to cloud microphysics, surface fluxes, and radiation processes in order to understand the variability and significance of these processes produced in a CRM. This is conducted by a number of GCE simulations of the GCSS WG4 case 2 (TOGA-COARE 19-27 Dec. 1992), as outlined in section 2. A study of this case has been performed by Petch and Gray (2001) for different versions of their microphysical scheme and sensitivities to radiational changes, as well as resolution and domain size. This study, however, differs in that it will incorporate four different microphysical packages to investigate specifically the role of warm rain processes, snow, ice, and graupel, represented by both low and high densities, for tropical deep convective systems, rather than variations of the same package (Swann, 1998) as was done by Petch and Gray (2001). In addition, this study will examine the effects that air-sea interactions play on the simulated tropical systems, using both the aerodynamic formulation and TOGA-COARE flux parameterization as discussed in the experimental results of section 3. A study of the response from domain size, resolution, and model numerics was already performed for this case by Johnson et al (2002), and thus will not be covered here. We believe it is important to include the GCE in this type of study in order to further understanding of the physical processes in CRM models. Therefore in section 4, we compare the GCE results to previous CRM studies of deep tropical convection of TOGA

COARE and other cases. Attempts are made to compare the results to observations when available. A discussion and summary of the results is given in section 5.

2. Numerical Experiments

A total of seven 2-D GCE simulations were conducted for the TOGA-COARE IFA region during the period 19-27 December 1992, in a manner similar to Part I (Johnson et al., 2002). The primary differences between the simulations were divided into three main areas including microphysics, surface, and radiation scheme as shown below in Table 1. The model domain size, grid spacing, and time step were identical for all simulations, and were set to the control simulation (C512). Thus the model domain size was 512 x 41 grid points, the grid spacing was $dx=1000$ m and $dz=80$ m near the surface, stretching to approximately 1100 m at the top of the domain, and the time step used was 6 s.

Simulation C512 is the same identical simulation described in Paper I (Johnson et al. 2002) and includes a full bulk microphysics parameterization, aerodynamic sea-air transfer fluxes, and full interactive radiation. The control simulation consists of a 512-km model domain with 1000 m horizontal grid spacing, 41 vertical grid points, a bulk surface flux formulation, shortwave and longwave radiation parameterizations (Chou 1984, 1986, 1990, 1992, 1994, 1999), and Rutledge and Hobbs (1984) three-category ice-phase scheme (cloud ice, snow, and graupel/hail). Further details of the GCE model are given in Tao et. al (1993) and Tao et al. (2003). The NOICE case consists of the GCE without ice microphysics implemented (only liquid water physics), 2 ICE is for a 2-ice scheme consisting of only cloud

ice and graupel, NOSFC is for a simulation without the incorporation of surface heat and moisture fluxes, TOGA for the implementation of TOGA-COARE surface fluxes, and NORAD for the exclusion of all radiation processes.

3. Results

3.1 *Sensitivities to surface fluxes and radiation*

The first set of experiments involve sensitivities involving surface fluxes and radiation by invoking the aerodynamic surface flux parameterization (case C512), the TOGA-COARE flux algorithm (TOGA), the full elimination of surface fluxes (NOSFC), and the removal of the explicit radiation parameterization (NORAD). A description of how these changes affect the thermodynamics, dynamics, cloud structure and precipitation in 2D GCE simulations of deep tropical convection is now examined.

3.1(a) Temperature and water vapor bias

The 8-day mean temperature and water vapor bias (from observations) for the surface flux cases and case without radiation is shown in Fig. 1. The NOSFC case mean temperature bias is near -6 K, which is approximately -4 K cooler than the cases that include surface fluxes, and this bias extends throughout the troposphere. The NOSFC case mean water vapor mixing ratio bias is also much greater than the other cases, with deficits increasing to -3.4 g/kg

near the surface. Thus the addition of latent heat transfer from the ocean to the atmosphere plays a major role in the significantly warmer and moister mean atmospheric temperatures and water vapor mixing ratios. The TOGA case produces smaller latent fluxes than the control case (Table 2) which results in mean tropospheric temperatures approximately 0.4 K cooler than C512 and slightly less moisture near the surface and mid troposphere. The effects of radiation (NORAD), at least during this active TOGA COARE multi-day period, have very little impact on the mean temperature and water vapor below 200 mb. However, above 200 mb, the NORAD case produces temperatures as much as 6K warmer than C512, which is a result of radiational cooling being eliminated. The 19-27 December 1992 TOGA COARE case produced a thick cloud layer during much of the period, and thus the radiational effects are primarily located near the tropopause with only small effects below 200 mb.

Figure 2 shows that the NOSFC case has significantly lower standard deviations of both temperature and water vapor throughout most of the troposphere, as the removal of air-sea heat and moisture transfer produces less variation in the thermodynamic state of the atmosphere. The TOGA case has slightly less variation in temperature and moisture as the fluxes are somewhat weaker than C512. The NORAD case produces the largest water vapor deviations near 950 mb (1.15 g/kg), showing that there is more low-level variation in moisture when radiation processes are excluded. This is likely due to greater evaporation and rainfall in the NORAD case as described later in this section. In addition, for the NORAD case near the tropopause, temperature deviations are largest of the four cases. Thus longwave radiational cooling has a modulating effect on temperature deviations near the cloud tops,

while the NORAD case temperatures are warmer and fluctuate more through latent heat release of ice and turbulence above the cloud tops.

Table 3 shows that the cooler and drier NOSFC case has a mean CAPE of only 212 compared to 700 for the control case. The mean CAPE for the TOGA case is 644 as surface fluxes are weaker than C512, but slightly greater than C512 for the NORAD case where low-level moisture and temperatures are slightly greater. Therefore convection can be expected to be slightly greater for the case without radiation, but much weaker when surface fluxes are excluded.

3.1(b) Vertical motion

Figure 3a shows the maximum and minimum vertical velocities at each level which are averaged throughout the entire simulation. There is good agreement between the cases C512, TOGA, and NORAD in average maximum updraft velocity throughout the troposphere, with peak mean updrafts near 4 m/s occurring between 600 and 800 mb. Conversely the NOSFC case produces maximum updrafts and downdrafts of only approximately 50-75% that of other cases, again indicating less intense convection when surface fluxes are eliminated. Maximum mean vertical downdrafts also show very close agreement between the control (C512) and TOGA cases with peak downdrafts of -2 m/s occurring between 600 and 800 mb, and -2.5 m/s at 150 mb. The NORAD case, however, produces increasingly weaker maximum downdrafts from 800 to 200 mb, which is due to the elimination of LW radiational

cooling from the cloud. Although maximum updrafts are similar between the NORAD and C512 cases, the mean updraft at each level and averaged with time (Fig. 3b), shows that the NORAD case produces much weaker mean updrafts and downdrafts overall (only 0.2-0.25 m/s vs. 0.4-0.5 m/s in C512 and TOGA cases). Therefore radiation processes have only a small effect on the intensity of convection, but play a significant role by approximately doubling the mean vertical air mass transfer. The mean vertical velocities of the NORAD case are even weaker than the NOSFC case, which has weaker mean updrafts and downdrafts below 400 mb compared to C512 and TOGA. Thus surface fluxes play a larger role in convection than in mean vertical mass transfer, which is significantly influenced by the large-scale forcings discussed in Johnson et al. (2002).

3.1(c) Cloud structure

The control (C512) and TOGA cases display three distinct peaks in cloud fraction near 150 mb (80%), 300 mb (40%) and 600 mb (15%) as shown in Fig. 4a. These regions are located in the cloud ice anvils, the graupel and snow layers, and the lower-level liquid clouds respectively. Although water vapor is greatly reduced, the mean cloud fraction, defined in Johnson et al. (2002), is actually greater when surface fluxes are removed (NOSFC) due to lower temperatures and greater relative humidities (Fig. 4b). The NOSFC case not only depicts a larger CF of 20% in the liquid layer, but the peak is at a lower level near 675 mb, which is due to weaker convection and level of saturation in this case. The NOSFC mean cloud fraction is also larger in the 300 mb (60%) and 150 mb (85%) regions, as relative

humidities are also higher in these regions. The NORAD case is nearly identical to C512 below 300 mb, but only possesses one upper-level peak near 180 mb, which has a lower intensity of only 65%. By removing LW radiational cooling near the cloud tops, temperatures are much warmer near 130 mb in the NORAD case (Fig. 1a), and clouds instead develop below these levels where relative humidities are higher (Fig. 4b). Therefore it is shown that radiational processes are necessary in order to produce the bi-modal cloud fraction peaks above 400 mb, which is more distinct when surface processes are eliminated. Petch and Gray (2001) also show significant changes in the cloud ice structure when radiation is excluded.

It is important to note that greater cloud fractions do not necessarily indicate more hydrometeor mass. Figure 5a shows that the NOSFC case does produce greater hydrometeor mass than C512 near 350 mb (0.11 vs. 0.08 g/kg), but the total mass is less than C512 near the 600-mb peaks (0.14 vs. 0.16 g/kg). This indicates that without surface fluxes, the model produces more cloudiness, but these clouds have smaller droplet diameters and masses (concentration of cloud droplets is fixed in these simulations). Smaller drop sizes also contribute to the lower maximum downdraft velocities in the NOSFC case as shown earlier in Fig. 3.

The horizontal domain mean contours of the total hydrometeor mixing ratio for the 8-day period are shown in Fig. 6. There are five maximums in hydrometeor mass between 20-27 December which lie near 570 mb for all the cases except for NOSFC, which lies at lower levels near 610 mb as the level of saturation is lower. The NOSFC case also depicts a 6th

hydrometeor maximum of 0.16 g/kg near the end of 19 December which is more distinct than the other cases, although hydrometers develop later that day than the other cases. The peak hydrometeor mass on 24 December is only slightly less in the NOSFC case (near 0.36 g/kg) than the other cases (0.38-0.42 g/kg), due to weaker convection. The similarity with the other cases, however, signifies the strong influence of the large-scale forcings on the overall mean cloud development. In general, the TOGA case hydrometeor fields are only slightly weaker but otherwise very similar to C512. The NORAD case structure is also similar to the control case, with the distinction of minimal hydrometeor mass above 200 mb due to removal of IR cooling near the tropopause, and somewhat greater hydrometeor mass near 300 mb.

The NOSFC case produces more distinct secondary peaks in hydrometeor mass near 300 mb during the stronger convective events on 21, 22, and 24 December. An explanation for this is that convection is weaker in the NOSFC case, and there is less vertical mass flux from the mid- to upper-levels as shown by the mean cloud mass flux in Fig. 5b. Here the peak mean updraft mass flux for case C512 ($1.25 \text{ kg/m}^2/\text{s}$), is located near the cloud base at 925 mb, while the peak downdraft mass flux is approximately $0.24 \text{ kg/m}^2/\text{s}$ and located in evaporative downdrafts near 800 mb. The cloud updraft mass fluxes have a secondary peak near 500 mb in regions of greater ice mass, where values reach 0.75 to $1.11 \text{ kg/m}^2/\text{s}$. The elimination of surface fluxes (NOSFC) has a dramatic effect on weakening cloud updraft mass fluxes to approximately 50% of C512 below 400 mb, and cloud downdraft mass fluxes below 600 mb as vertical motions (Fig. 3) are weaker. The NORAD case also has a significant impact on increasing cloud updraft mass fluxes by 10-20%, and decreasing cloud downdraft

mass fluxes above 800 mb by up to 50% since downdrafts from LW cooling have been eliminated.

Therefore there is a greater discontinuity in the liquid and ice layers when surface fluxes are excluded. The NORAD mass flux is also greater than the other cases from 350 to 500 mb, resulting in greater upward transport of ice mass shown in Figs. 5 and 6. Note that the smaller drop sizes in the NOSFC case is also resulting in smaller mean downward cloud mass flux below 600 mb in NOSFC compared to the other cases.

Evidence of the weaker convection in the NOSFC case is depicted by X-Z cross-sections of the total hydrometeor fields during an active period (18 Z 24 December 1992) shown in Fig. 7. Here it is evident that the NOSFC case has greater cloud cover, and much weaker convective cells extending to only 400 mb, which is overridden by an ice layer aloft near 300 mb. Convective cells in the other cases extend up to the tropopause and have typical sizes ranging from 10-30 km. It can also be seen that the NORAD case has cloudiness and cells extending to only 150 mb due to much warmer temperatures at these levels. In addition, the NORAD case has a greater number of convective cells, although they tend to be somewhat weaker than those in the C512 and TOGA cases.

3.1(d) Precipitation and its characteristics

Table 4 shows the total mean rainfall along with the fraction of the total rainfall which fell in convective and stratiform regions. As discussed in Johnson et al. (2002), the control case produces a mean total rainfall of 160.5 mm, which is in good agreement with the observed total rainfall of 160.8 mm. Slightly more than half of this rainfall (53.4%) came from convective regions, which agrees with other tropical cases over the western Pacific as discussed by Tao et al. (2000). The total rainfall, as well as the proportion which is convective is directly related to the intensity of the surface flux. The TOGA case, which has slightly weaker fluxes than C512, produces 1.2 mm less precipitation, and has 3.2% less convective rainfall. Meanwhile, the NOSFC case has only 134 mm of total rainfall, or 26.5 mm less than C512, of which only 30.7% is convective (22.7% less than C512). As already mentioned, the NOSFC case produces much less convection than the other cases and has a greater stratiform layer as shown in Fig. 7, even though the large-scale advective forcings primarily control the mean atmospheric heating and moistening. The NORAD case produces 2.6 mm more rainfall than C512, although the convective amount is proportionally the same. Therefore radiation processes have minimal effects on the precipitation amounts. This can be explained by the fact that radiation for this case primarily effects the heating and cloud structure in the upper troposphere due to the thick cloud layer and deep convection over the western Pacific during this TOGA event.

3.1(e) Heat and moisture budgets

Tables 5 and 6 show the total time-domain integrated temperature and moisture budgets for the control, surface flux, and radiation cases, in a manner similar to Johnson et al. (2002; tables 5 and 6). Although surface fluxes are eliminated in the NOSFC case, the net radiative heating of 24.6 W/m^2 is similar in magnitude to the control case (C512) sensible flux and radiational heating combined. Thus the cooler mean atmosphere shown in Fig. 1a is not a direct result of the removal of heat from sensible fluxes. However, the mean heating due to microphysical processes of 606.5 W/m^2 is significantly less than the control case (719.3 W/m^2). In addition, the atmospheric drying due to net condensation (-482.8 W/m^2), while much less than C512 (-579.40), does not offset the 161.2 W/m^2 latent flux from the ocean in C512. Thus the elimination of moisture fluxes from the ocean into the atmosphere reduces the net condensation in the NOSFC case to only about 84% that of C512, as the moisture is only supplied by the mean thermodynamic forcings discussed in Johnson et al. (2002). Therefore, the drier atmosphere in the NOSFC case (Fig. 1b) is a direct result of removal of latent fluxes, while the cooler atmosphere is primarily a result of the significant reduction of net condensation due to less moisture transfer from the ocean.

In the TOGA case, the surface fluxes of 19.0 W/m^2 are 4.2 W/m^2 smaller than those of C512, which uses the aerodynamic formulation. More notably, the latent heat flux in the TOGA case is 130.8 W/m^2 compared to 161.2 W/m^2 in C512, or a 19% reduction. However, from Fig. 1b, it can be seen that the mean moisture is up to 0.5 g/kg less in the TOGA case in only the lowest 50 mb and similar to C512 for the remainder of the troposphere. In addition, net condensational drying of the atmosphere is only 4.5 W/m^2

less than C512 overall. The reduction of net condensational warming in the TOGA simulation of 5.8 W/m^2 is resulting in a 0.2 K smaller mean temperature compared to C512, while an approximate 0.1 K reduction is due to the smaller sensible heat fluxes, shown in Fig. 1a. Overall the cooler mean atmosphere in the TOGA case is allowing for higher relative humidities (Fig. 4b), and greater condensation than if temperatures were warmer. Thus, even with a nearly 20% reduction in latent fluxes, the net impact on the mean moisture (Fig. 1b) and cloudiness (Fig. 5a) of the TOGA case is minimal compared to C512.

Overall the impact of removing explicit radiational heating/cooling has small direct impact on the mean temperature and moisture budgets since the mean radiational cooling in C512 is small (-1.9 W/m^2). The NORAD case does have greater condensational heating (11.0 W/m^2) and drying (8.8 W/m^2), mainly due to removal of radiational warming in the cloud layer of up to 0.4 K between 250 and 400 mb (Figs. 1a, 5a). Latent heat fluxes of 155.0 W/m^2 are also slightly smaller than C512 (161.2 W/m^2) due to removal of low-level SW warming. However the impact of this reduction on a mean basis is minimal and explicit radiational impacts are primarily found above 400 mb.

3.2 *Sensitivities to microphysical processes*

The second set of simulations involve sensitivities of the thermodynamics, dynamics, cloud structure, precipitation, and budgets for simulations involving different microphysical packages incorporated into the GCE, in a manner similar to the surface flux and radiation

sensitivities discussed in the previous section. Further discussion of the setup for these simulations can be referenced in section 2.

3.2(a) Temperature and water vapor bias

The 8-day mean temperature and water vapor bias (from observations) and standard deviations for the cases involving changes in microphysics are shown in Figs. 8 and 9. Below the melting layer near 600 mb, all the cases, with the obvious exception of the NOMLT case, have similar temperature deviations ranging from -1.2 to -2.0 K. The NOMLT case has significantly warmer temperatures which increase downward to a 0 K bias at the surface. The warmer low-level temperatures are a result of the additional heat gained by the removal of cooling due to melting, and increasing low-level depositional growth on the ice particles. Even so, there is less net transfer of water vapor to the hydrometeors below 900 mb, which is resulting in water vapor mixing ratios of 1 g/kg greater near the surface in the NOMLT case, and less overall precipitation (see section 3.2d). Above 900 mb, the NOMLT case has slightly less water vapor than the other cases due to greater sublimation of ice in the drier mid-levels. The removal of cooling due to melting in the NOICE case results in warmer temperatures below the melting layer by about 0.25 K, but greater evaporation and water vapor mixing ratios by approximately 0.2 g/kg than in C512. Meanwhile, the 2ICE case is nearly identical to the C512 case in both temperature and moisture throughout the troposphere, which indicates the insignificance of the third ice species (snow) on the overall mean thermodynamic state of the atmosphere in these multi-day tropical cases.

Above the melting layer at 600 mb the NOICE case becomes significantly cooler than the control case (up to -2 K), which is a result of the elimination of latent heat release of ice deposition. However above 200 mb, the mean temperature bias increases to 7 K from warming in and below the upper cloud layer, and then -27 K, due to much greater LW radiational cooling above the thick clouds consisting of liquid water. The larger ice hydrometeors play a significant role in the mid-level thermodynamic atmospheric state, while smaller ice particles play a crucial role in the radiational effects, especially near the cloud tops.

Figure 9a shows that the NOMLT case has standard deviations in temperature of only about half that of the other cases near the surface, which indicates increased fluctuations in temperature associated with wet-ice processes. In the mid-levels, the NOICE produces slightly smaller deviations in temperature with the removal of ice processes. However greater variations in temperature for the NOICE case does occur above the cloud layers where radiational cooling effects are strongest. Again the 2ICE deviations are similar to the control case, with slightly increased variation near 400 mb where the third ice species, graupel, exists in C512. Therefore, it is shown that the standard deviations in atmospheric thermodynamic state increase with increasing complexity of the microphysical scheme, and when water droplets exceed their natural heights, by being located near the tropopause in the NOICE case.

The standard deviations for water vapor, shown in Fig. 9b, are similar between the cases below the melting layer at 600mb, but there is an approximate 50% increase (0.4 to 0.6 g/kg) near the melting level (600 mb) for the cases 2ICE and C512. This is associated with the moisture variations associated with deposition/sublimation of numerous ice particles in these cases. The moisture deviations again reach a peak of 1.0 g/kg near 950 mb, where rainfall evaporation is at a maximum. The moisture deviations are similar between the cases near the surface, even though the NOMELT case has significantly weaker surface fluxes (Table 7).

An examination of the mean CAPE values (Table 8) shows that the NOMLT case has a much larger CAPE of 1845, primarily due to much larger near-surface temperatures and moisture as shown in Fig. 8. The NOICE simulation mean CAPE of 1091 is significantly higher than C512 as low-level temperatures and moisture are greater, but significantly cooler temperatures exist in the mid-levels as mentioned above. This leads to greater convection overall in the NOICE case as is discussed below.

3.2(b) Vertical motion

The time-averaged maximum updraft and downdraft velocities at each level are shown for all the simulations involving changes in microphysics in Fig. 10a. The most notable feature is the smaller upward vertical velocities of 2.5 m/s in the NOMLT case vs. 3.5-4.0 in the other cases from 500-900 mb. This is a result of greater precipitation loading of the

updrafts in the NOMLT case due to larger ice particles which do not melt. The NOICE and 2ICE schemes also produce mean maximum updrafts of approximately 0.5 m/s greater than C512 below 300 mb. There is less variation in maximum mean downdrafts, which range between -1.2 and -2.0 between 600 and 800 mb. The removal of graupel in the 2ICE case is resulting in smaller maximum downdrafts than the other cases. Another feature is the weaker maximum updrafts/downdrafts for the NOICE case near 200 mb as the updrafts extend to lower levels when ice is removed.

An examination of the mean vertical motions at each level for the entire simulation (Fig. 10b) shows that the control case (C512) and the 2ICE simulation have nearly identical mean vertical motions approaching 0.4 m/s, while the NOICE case is only about half (0.2 m/s) of this mean vertical flow. Since maximum updrafts for the NOICE case are similar or even exceed the control case, this would imply a larger region of non-activity and fewer convective cells when ice is excluded. The NOMLT case has mean vertical velocities which lie between the NOICE and C512 cases near 0.3 m/s. This would suggest that this case has weaker vertical circulations apart from the central updraft cores as well. Thus it is evident that ice processes alone can have a significant impact on the mean vertical circulations in warm tropical environments.

3.2(c) Cloud structure

Figure 11a shows the 8-day mean cloud fraction for the cases with different microphysical schemes. Similar to that discussed in section 3.1, the control and 2ICE simulations have the three distinct peaks in cloud fraction near 150, 300 and 600 mb (ice, snow/graupel, and water regions). The most evident feature is the huge anvil of liquid water in the NOICE case, which extends from 500 to 100 mb, with peak cloud fractions of 80-82% from 100-300 mb. This is associated with much greater relative humidities of approximately 90% up to near 100 mb (Fig. 11b) due to evaporation of liquid water rather than sublimation of ice. In addition, the NOICE case does not have any secondary peaks in cloud fraction at 600 mb as the liquid hydrometeor mass is transported vertically to the anvils of the storm where there is a tendency for it to remain. The NOMLT case is nearly identical to C512 and 2ICE above the melting layer, but has a smaller cloud fraction peak of 10% in the cloud water region, which is also at a higher level of 570 mb compared to 600 mb for the other cases. Since melting is not allowed, the cloud water is much less below 600 mb in the NOMLT case, and cloud fractions are only about half that of the other cases. In addition, the mean relative humidity in the NOMLT case is $< 80\%$ near 800 mb (Fig. 11b) as less evaporational cooling is occurring and temperatures are warmer (see Fig. 8a).

An examination of the 8-day mean total hydrometeor mixing ratio (Fig. 12a) and domain-averaged contours of the total hydrometeor mixing ratio (Fig. 13) reveals several interesting features. Perhaps most notably, the large anvil of liquid water in the NOICE case, which reaches 0.46 g/kg at 225 mb, and the anvil of snow in the 2ICE case extending to 0.32 g/kg near 500 mb. The mean cloud mass flux (Fig. 12b) shows a spike in the 2ICE mass flux

of $1.1 \text{ kg/m}^2/\text{s}$ near 500 mb, indicating that the snow is being carried upward and into the anvils and does not significantly effect precipitation at the surface. This peak is nonexistent in the NOICE case. Petch and Gray (2001) also show secondary peaks in the convective mass flux which is dependent on both the microphysical parameterization, and the dimensionality of the simulation. In the NOICE case, the liquid water anvil exists throughout the period as shown on Fig. 13. Since much of the water is being transferred to the upper levels, less water is reaching the surface than in the C512 case. In addition, the NOICE case does not exhibit the cloud water hydrometeor peak near 600 mb. Although the 2ICE case has greater hydrometeor mass just above the freezing level, the mass just below and to the surface is nearly identical to the control case (C512). Thus about the same ice mass is melting into rainwater for both the 2ICE and C512 cases. However, the 2ICE has larger anvils of snow, which would have significant impact on the mid-level radiational heating for that case.

Note that below the freezing level at 600 mb, all the cases have a similar linear decline in total hydrometeor mixing ratios as the hydrometeors are evaporating in the lower-level atmosphere shown in Fig. 12a. It is evident that less hydrometeor mass, or rainwater, is reaching the surface in the NOICE case (0.03 g/kg) than in C512 (0.04 g/kg). The NOMLT case has much greater hydrometeor mass near the surface, which is largely composed of graupel mass. Since the fall velocity of small graupel particles is less than rain water, the surface precipitation rate is not proportionally higher in the NOMLT case. The greater low-level hydrometeor mass coverage in the NOMLT case is also seen in the mean contour plots (Fig. 13).

X-Z cross-sections of the total hydrometeor mixing ratio during the convectively active event of 18 Z 24 December 1992 is shown for all the cases involving microphysical sensitivities in Fig. 14. The NOICE case again shows a solid layer of liquid water above 300 mb which extends throughout the domain. Convective cells in this case extend only up to the base of this layer near 300mb, thus transporting much of the water mass upward from the lower levels. Much of this rainwater then evaporates below the anvils away from the main convection. The 2ICE case also depicts a layer of snow in the 200-500 mb region with some penetration of the convective cells through this layer to the upper troposphere. The remaining two cases have deep convection throughout the troposphere. However, there is greater westward vertical tilt of the convective cells in the NOMLT case as the updrafts/downdrafts are significantly weaker than C512. The NOMLT case also has more coverage of hydrometeor mass throughout the domain which is due to slower falling snow and small graupel particles below the melting layer. Therefore it is shown that melting plays a significant role in both the distribution of hydrometeor species, and on the dynamics of the storm, even though large-scale advective forcings and momentum are actively applied to the model.

3.2(d) Precipitation and its characteristics

Table 9 shows the total mean rainfall and percentage which is convective and stratiform over the entire 8-day simulation for the four cases involving microphysical processes. Although much of the snow in the 2ICE case is advected into the anvils, some

melts which leads to slightly greater rainwater mass below 600 mb and total precipitation of 161.7 mm (vs. 160.5 for C512). The larger anvils in the 2ICE case results in a reduction of convective rainfall to 50.9% from C512. The NOICE case produces the least surface precipitation of 151.6 mm, which is due to the greater transport of water mass away to the anvils above 300 mb, and evaporation below the anvils. However, the precipitation that does fall tends to be more concentrated, which lead to the greatest proportion of rainfall which is convective (62.5%) of all the cases in this study. Finally, although the NOMLT case has a greater low-level hydrometeor mass than that other cases, the total surface precipitation is 7.8 mm less than C512 as the terminal velocity of ice particles is much less than liquid drops, leading to a covering of hydrometeors throughout the domain as shown in Fig. 14. This also greatly reduces the convective precipitation in the NOMLT case to only 23.6% compared to 53.4% in the control case (C512). Tao et al. (1995) also found only minor changes in surface precipitation when melting processes were removed in a tropical squall case, although significant differences in precipitation were seen in a midlatitude squall.

3.2(e) Heat and moisture budgets

Tables 10 and 11 show the domain-time integrated temperature and moisture budgets for the five microphysical cases, in a manner similar to that described in section 3.1(e). Significant differences in the temperature and moisture budgets are seen for the NOICE, and NOMLT cases from the control case C512, and less so with the 2ICE case. The NOMLT case has weaker sensible and latent heat fluxes from the surface which is due to weaker downdrafts

as shown in Fig. 10, and significantly greater low-level temperatures and moisture as shown in Fig. 8. The removal of cooling due to melting is contributing to 21.4 W/m^2 greater microphysical warming in the NOMLT case (compared to C512). In addition, the warmer low-level temperatures are due to less net evaporation/sublimation below the melting level at 600 mb, resulting in lower relative humidities (Fig. 11b) and greater microphysical heating. There is an addition of moisture to the atmosphere equivalent 30.9 W/m^2 due to microphysical processes, however, much of this additional moisture is located below 900 mb in the moist boundary layer. The weaker vertical velocities in the NOMLT simulation is also leading to greater moisture and warmer temperatures entrapped in the boundary layer below 950 mb. The less dense snow hydrometeors can at times exist throughout the domain (Fig. 14), and there is greater net radiational cooling in the NOMLT case, which offsets the net microphysical warming.

The NOICE case has a net cooling of 16.7 W/m^2 from the C512 case with the majority of this difference coming from a net reduction in microphysical heating. An examination of Fig. 8a shows that large changes in the mean temperatures occur above 100 mb due to longwave cooling, and near 150 mb due to radiational warming in the thick upper cloud layer. However the net radiational cooling is a mere 0.43 K when integrated over the entire domain for the 8-day simulation. The overall cooler simulation for the NOICE case is a result of cooling between 250 and 500 mb of up to 2K due to the removal of ice depositional processes. The overall net moisture budget is nearly unchanged from C512 as net microphysical moistening of 3.7 W/m^2 is nearly balanced by decreased surface latent heat

fluxes of 5.1 W/m^2 . Mean vertical velocities (Fig. 10b), however, are much weaker in the NOICE case, and there is less transfer of heat and moisture vertically in the NOICE case. Therefore Fig. 8 shows a warmer and moister troposphere below 700mb when compared to the control (C512) case.

Finally, the 2ICE case temperature and moisture budgets are closest to the control case (C512) for all the simulations involving microphysical changes. Table 10 shows that there is slightly greater heating due to microphysics (7.0 W/m^2), radiation (4.0 W/m^2), and surface sensible fluxes (1.2 W/m^2). The contributions of all three occur at different levels of the atmosphere, and the result is a mean temperature profile (Fig. 8a) which is overall similar to C512. The water vapor budget shows a slightly drier atmosphere in the 2ICE, due to slightly greater net condensation/deposition (-5.0 W/m^2), and less latent heat flux (-0.9 W/m^2). Therefore it is demonstrated that the additional graupel ice species has only little impact on the mean thermodynamic state of the atmosphere, at least for this case of deep tropical convection in the western Pacific.

4. Comparisons with previous studies

Several multi-day CRM modeling studies incorporating cyclical boundaries, large-scale advective forcings, and relaxed large-scale momentum, have been performed recently by modelers for convection in tropical regions. Here we analyze the results from our study to previous multi-day CRM simulations in similar environments and model configurations, in

order to compare and contrast our results in terms of sensitivities to microphysics and radiation with these previous studies.

4.1 *Microphysical processes*

Petch and Gray (2001) performed a CRM study of this same TOGA COARE case, but from the period 00 Z 20 December – 00Z 26 December 1992, using the Met Office Large-Eddy Model described by Shutts and Gray (1994), and Gray (2000). Their results also showed that the strength of convection was only minimally changed with different microphysical packages, and there was a secondary peak in the total hydrometer content near 10 km similar to our control case. They did not show a secondary peak in the updraft convective mass flux for the 2D simulations, which contrasts with the Rutledge-Hobbs microphysical package in our study showing a secondary peak near 400 mb (Fig. 12). The NOICE case, however, did not exhibit the secondary peaks. There is a significant difference between the daily precipitation rates for the 2D cases in Petch and Gray (15.0 mm/day from Table 4), and this study for the same 6-day period (22.9 mm/day). This indicates the significance of how microphysical processes are represented in the CRM. It should be noted that the mean observed precipitation rate was approximately 21.5 mm/day during the 6-day period. In addition the different ice microphysical simulations in this study produced greater changes in the cloud mass fluxes and hydrometeor mixing ratios than did the changes in microphysics in Petch and Gray. This is likely attributed to the more radical changes of ice microphysics in this study (e.g. removal of graupel and melting processes) compared to Petch and Gray.

Wu et al. (1998), using the Clark-Hall cloud model (Clark et al. 1996) ran the TOGA-COARE in two –dimensions for 39 days (5 December 1992 – 12 January 1993). Their results showed that the thermodynamic fields and budgets were well simulated in periods of strong convection (strong forcings). However, they also show a net cooling of 1-2 K during the active period, along with net moistening in the mid levels as was the case in this study. Other CRMs in the GCSS WG4 have also reported similar excessive cooling near 2 K throughout the troposphere (Krueger and Lazarus, 1999), which is likely a consequence of errors in the sounding instruments used during TOGA-COARE (Wu and Moncrieff, 2000). They also showed that during convective periods, the downdraft mass flux is about half the updraft mass flux in the lower half of the troposphere which is similar to our results in Figs. 5 and 12. This reinforces the importance of including downdrafts in parameterization schemes.

Another key find in Wu et al. (1998) is that the cloud (ice and liquid) water contents were too large, which was attributed to the cyclical boundaries and the absence of observed data to specify large-scale forcings for the condensed water. Grabowski et al. (1996) has noted similar results in a 7-day simulation of GATE cloud systems. The GCE simulation did not have strong evidence of excess cloudiness in this TOGA COARE case, although a previous study did show excessive cloudiness when the domain size was less than 512 km (Johnson et al., 2002). Therefore we conclude that the microphysical parameterization utilized in the CRM should also be considered as major contributor to the excess cloudiness in a periodical lateral boundary setup.

Wu et al. (1999) simulated the same 39-day TOGA COARE case, but with a modified ice scheme more representative of ice pellets and frozen droplets instead of dendritic or columnar ice crystals. In addition, a nonlocal boundary layer diffusion scheme was included. Their results showed better 39-day domain-mean thermodynamic differences from observed using the modified ice scheme. In our study, the C512 and NOICE case had similar mean atmospheric thermodynamics although drastic differences are noted in the NOICE case. However a case using the Lin et al. (1983) microphysical scheme did produce noticeable changes in the mean thermodynamic state compared to C512 (not shown). Wu et al. (1999) showed very small differences in mean precipitation and convective intensity between the original and modified ice scheme which is in agreement with our study between C512 and 2ICE. They also showed a much smaller ice water path with the modified ice scheme. Our study also has similar convective intensities between C512 and 2ICE (Fig. 10), and shows a much smaller ice mass in C512 compared to 2ICE (Fig. 12a) in the mid-levels, due to the conversion to larger graupel particles which have greater terminal velocities compared to snow. McCumber et al (1991) also shows better structure of simulated tropical convection when ice categories are increased. The sensitivities of the mean cloud properties to microphysics indicates that more microphysical observations are needed to understand the physical processes involved in deep tropical clouds.

Grabowski et al. (1999) performed a number of 7-day simulations forced by evolving large-scale conditions based on GATE observations, to study the effects of cloud

microphysics on the convecting tropical atmosphere. A key finding was that the cloud microphysical processes affected the moisture and temperature regimes in such a way that relative humidity profiles changed little. Our study also showed small differences in relative humidity between the 2ICE and C512 cases, and NOMLT case above 600 mb. The more radical case without ice processes (NOICE) showed much larger relative humidities above 600 mb due to the large transport of water mass aloft. Grabowski (2003) shows a similar feature when using the Berry (1968) formulation of the warm-rain autoconversion term, and was able to reduce this transport by replacing the autoconversion term with Kessler's (1969) formulation. Similar to Grabowski (2003), we found that without ice (NOICE), the systems had a reduced stratiform component and shorter life cycle than mesoscale systems with ice microphysics included. However, the NOICE case was able to produce the main dynamic features of the system, which is a characteristic of environments with strong convective instabilities (Liu et al., 1997).

Tao and Simpson (1989) ran two-dimensional simulations of a GATE squall line using the GCE model with and without ice processes included. Their results showed that the outflow structure is generally determined by the water loading and evaporative cooling by rain. Thus the cold outflow structure in the leading edge of the convective region was not significantly affected by ice-phase microphysical processes. This study also showed only small differences in mean maximum updraft and downdraft velocities in the low- to mid-levels of the troposphere. Tao and Simpson (1989) also showed that when ice was excluded, 88.5% of the total rainfall came from convective regions, versus 67.3% when ice is included.

Although the study in this paper involved a long-term simulation of cloud ensembles, we also show a significant increase in convective rainfall (from 53.4% to 62.5% in Table 9) when ice is excluded. Similar to Tao and Simpson (1989) the ice-free case in this study also has a reduction in the depth of the stratiform cloud and the clouds have more cellular rather than mesoscale features.

Forvell and Ogura (1988) simulation of a midlatitude squall line found that the scale features were too narrow in the convective region, producing heavier precipitation over a smaller distance from the gust front compared to observations. In addition, the total precipitation without ice processes was 8.8% less than when ice processes was included. Our study also shows a reduction in rainfall (5.5%) when ice processes are excluded and a more concentrated and heavier rainband.

4.2 *Radiation processes*

A difference between Petch and Gray (2001) and our study is that the elimination of explicit short- and long-wave radiational processes resulting in slightly greater updraft mass fluxes and ice mixing ratios in the GCE simulation for NORAD (Fig. 5), as well as total precipitation, while the opposite was the case for Petch and Gray (2001). This may be a result of the radiation and microphysical parameterizations utilized in each model, however both studies showed that the large-scale forcings are the dominating influence, and explicit radiational effects are secondary in nature. However, again the mean vertical velocities were

much weaker when explicit radiation was excluded, as shown in Fig. 3b. Our results, as with Petch and Gray (2001), did show the strongest impact of radiation above 8 km, where radiation dominated over the large-scale forcings of the simulation. However, we did not find that explicit radiation had as large an impact on the simulation.

The total precipitation for the NORAD case was slightly greater than C512, while the structure of the cloud systems were minimally effected. This is in agreement with previous studies showing reduction of precipitation and small effects on overall cloud structure when radiation processes are included (e.g. Chin et al., 1995). Tao et al. (1996) showed that longwave cooling at the cloud tops and warming at cloud base did enhance circulations in the cloud regions, which was also the case in this study. Xu and Randall (1995) and Fu et al. (1995) suggested that the longwave cloud-top cooling and cloud-base warming destabilization mechanism could be important for prolonging the lifespan of high anvil clouds (around 10 km), which was shown also in this study (Figs. 6 and 7). Xu and Randall (1995) showed that this direct cloud destabilization does not have any impact on surface precipitation as well. Sui et al. (1998) used the GCE model and performed a 15-day integration to simulate TOGA COARE convective systems. One of their key conclusions was that the nocturnal rainfall maximum (1300-1400 UTC) is related to IR cooling and a greater relative humidity and precipitable water at night. The GCE-simulated results also show a peak in the hydrometeor mass near 1400 UTC (Fig. 6), which is primarily a response to the large-scale advective forcings as the radiational contributions have only small effects on mean hydrometeor mass.

5. Summary and conclusions

This study examined the sensitivities of surface fluxes, explicit radiation, and microphysical processes in 8-day simulations of deep tropical convection over the western Pacific using the GCE model. The simulations incorporated large-scale advective potential temperature and moisture forcings updated every time step, as well as large-scale momentum, in a semi-prognostic manner (Soong and Tao, 1980; Tao and Soong, 1986; and many others) on a periodic lateral boundary domain.

The major results can be summarized as follows:

- The removal of surface fluxes produced a much cooler (4 K) and drier troposphere (up to 2.5 g/kg), and much smaller CAPE. This led to a 10% reduction in total rainfall (compared to case C512), 50% greater stratiform coverage, and much less convection in general. The weaker convection contributed to maximum vertical velocities and cloud mass fluxes that were approximately 50-60% that of the other cases.
- For the simulation using the TOGA-COARE surface flux algorithm, the surface fluxes were approximately 10% weaker than C512 but closer to observations taken from the IMET buoy. The same trends in mean thermodynamics, vertical velocities, cloud coverage, and convection were found as in the NOSFC case, but to a much lesser extent.

- The elimination of explicit shortwave and longwave radiation was found to have only minimal effects on the mean temperature and moisture budgets, mean precipitation in both convective and stratiform regions, cloudiness below 400 mb, and mean budgets overall. However, the removal of radiation processes led to much warmer temperatures above 200 mb, which eliminated cloudiness and greatly affected the cloud structure near the tropopause. In addition, mean vertical winds were only 50-60% as strong as C512, as diurnal low-level warming, and upper-level radiational cooling was eliminated. These conclusions agree with a study of the same case by Petch and Gray (2001), with the exception that precipitation was weaker when radiation was excluded in their case. It should be noted that radiational processes have been fractionally incorporated within the advective and momentum forcings utilized in these cases.
- The removal of ice processes had major impacts on the mean thermodynamic atmospheric state, mean vertical velocities, cloud structure, and convective precipitation. The greatest effects were above 400 mb, where anvils of supercooled liquid water existed. This water was transported away from the lower levels, which led to 9 mm less precipitation than the control case (C512). However, the precipitation that fell was in a more concentrated band, leading to 9% greater convective rainfall than C512. Temperatures above the anvils in the NOICE case were much cooler due to strong radiational cooling, but much warmer near 150 mb in the cloud layer. In addition, there were weaker mean vertical velocities due to the removal of sublimation and melting.

- The removal of graupel physics produced results similar to C512 in terms of mean thermodynamics and vertical velocities. The cloud structure was different in that there was a large anvil of snow near 550 mb which had a mass about three times as large as C512. However, the mean hydrometeor mass below 600 mb was similar to C512, due to the low terminal velocities of snow compared to graupel. Overall the total rainfall was only 1.2 mm greater than C512, and convective rainfall only 2.5% less. Therefore in this case of deep tropical convection in the western Pacific, it is demonstrated that the graupel species plays only a secondary role in the mean temperature and moisture budgets on a multi-day scale.
- The removal of melting processes had major impacts on the thermodynamics, dynamics, and hydrometeor structure below the melting level (600 mb). There was less evaporation and lower relative humidities in the 600-900 mb region. Temperatures near the surface were 2 K warmer due to removal of cooling due to melting. In addition, a much moister boundary layer, fed by rapidly sublimating ice particles, contributed to a CAPE nearly three times greater than C512. However, there was also a greater dispersion of graupel and snow hydrometeors throughout the domain, leading to a convective portion that was reduced by a factor of 2 (to 23.6%). The larger cloud cover contributed to greater net radiational cooling, but much weaker surface fluxes, due to the warm, moist boundary layer, led to only small changes in tropospheric mean temperature and water vapor from C512, and an over overall total precipitation reduction of only 7.8 mm.

The results in the NOMELT case differ from an EMEX squall line case by Tao et al. (1995), where they found that squall development was not sensitive to the presence of melting, due to the dominance of warm rain processes, although a simulated PRE-STORM midlatitude continental squall line structure was largely affected by melting ice. They also found a 6% increase in surface precipitation when melting processes were eliminated, while this study had a 5% decrease in surface precipitation. These differences may be due to the fact that a well organized squall line was simulated in Tao et al. (1995), and/or that the study had a much shorter time integration in Tao et al.

A number of comparisons were made between the results of this study involving the sensitivities in microphysics and radiation, and with previous CRM studies in similar tropical environments. Both similar and different trends were noted in thermodynamics, cloud structure, and precipitation, between the GCE and other CRMs. Overall, microphysical processes had the strongest impact in these trends below 8 km, while radiation had the largest influence at the cloud anvils and aloft.

It should be noted that many of the results in this study are case specific and caution must be given in applying these results to other tropical cases, or cases in different locales. In addition, an examination of the cloud structure or budgets (e.g. radiation) on a shorter time scale would produce results much different from observational "truth". Finally clouds and tropical convective systems are three-dimensional in reality, but good statistical agreement can be found between the multi-day 3-D and 2-D studies in this case due to the strong influence of

the large-scale advective forcings and momentum. However, we do plan and are in the process of performing simulations of this and other cases using the 3-D GCE model.

6. Acknowledgements

This work is mainly supported by the NASA Headquarters Atmospheric Dynamics and Thermodynamics Program and the NASA Tropical Rainfall Measuring Mission (TRMM). The authors are grateful to Dr. R. Kakar at NASA headquarters for his support of this research. Acknowledgment is also made to the NASA/Goddard Space Flight Center for computer time used in this research.

7. References

- Chin, H.-N. S., Q. Fu, M. M. Bradley, and C. R. Molenkamp, 1995: Modeling of a tropical squall line in two dimensions and its sensitivity to environmental winds and radiation. *J. Atmos. Sci.*, **52**, 3172-3193.
- Chou, M.-D., 1984: Broadband water vapor transmission functions for atmospheric IR flux computation. *J. Atmos. Sci.*, **41**, 1775-1778.
- Chou, M.-D., 1986: Atmospheric solar heating rate in the water vapor bands. *J. Climate Appl. Meteor.*, **25**, 1532-1542.
- Chou, M.-D., 1990: Parameterization for the absorption of solar radiation by O₂ and CO₂ with application to climate studies. *J. Climate*, **3**, 209-217.
- Chou, M.-D., 1992: A solar radiation model for use in climate studies. *J. Atmos. Sci.*, **49**, 762-772.
- Chou, M.-D., and M. J. Suarez, 1994: An efficient thermal infrared radiation parameterization for use in general circulation models. NASA Tech. Memo. 104606, Vol. 3, 85 pp.
- Chou, M.-D., and M. J. Suarez, 1999: A shortwave radiation parameterization for atmospheric studies. NASA Tech. Memo. 104606, Vol. 15, 40 pp.
- Clark, T. L., W. D. Hall, and J. L. Coen, 1996: Source code documentation for the Clark-Hall cloud-scale model: Code version G3CH01. NCAR Tech. Note NCAR/TN-426+STR, 137 pp. [Available from NCAR Information Service, P. O. Box 3000, Boulder, CO 80307.]
- Donner, L. J., C. J. Seman, and R. S. Hemler, 1999: Three-dimensional cloud-system modeling of GATE convection. *J. Atmos. Sci.*, **56**, 1885-1912.
- Fovell, R. G., and Y. Ogura, 1988: Numerical simulation of a midlatitude squall line in two dimensions. *J. Atmos. Sci.*, **45**, 3846-3879.
- Fu, Q., S. K. Krueger, and K. N. Liou, 1995: Interactions of radiation and convection in simulated tropical cloud clusters. *J. Atmos. Sci.*, **52**, 1310-1328.
- Grabowski, W. W., X. Wu, and M. W. Moncrieff, 1996: Cloud resolving modeling of tropical cloud systems during PHASE III of GATE. Part I: Two-dimensional experiments. *J. Atmos. Sci.*, **53**, 3684-3709.

- Grabowski, W. W., X. Wu, M. W. Moncrieff, and W. D. Hall, 1998: Cloud-resolving modeling of cloud systems during phase III of GATE. Part II: Effects of resolution and the third spatial dimension. *J. Atmos. Sci.*, **55**, 3264-3282.
- Grabowski, W. W., X. Wu, and M. W. Moncrieff, 1999: Cloud resolving modeling of tropical cloud systems during phase III of GATE. Part III: Effects of cloud microphysics. *J. Atmos. Sci.*, **56**, 2384-2402.
- Grabowski, W. W., 2000: Cloud microphysics and the tropical climate: Cloud-resolving model perspective. *J. Climate*, **13**, 2306-2322.
- Grabowski, W. W., 2003: Impact of ice microphysics on multiscale organization of tropical convection in two-dimensional cloud-resolving simulations. *Quart. J. Roy. Meteor. Soc.*, **129**, 67-81.
- Gray, M. E. B., 2000: Characteristics of numerically simulated mesoscale convective systems and their application to parameterization. *J. Atmos. Sci.*, **57**, 3953-3970.
- Johnson, D. E., W.-K. Tao, J. Simpson, and C.-H. Sui, 2002: A study of the response of deep tropical clouds to large-scale thermodynamic forcings. Part I: Modeling strategies and simulations of TOGA COARE convective systems. *J. Atmos. Sci.*, **59**, 3492-3518.
- Krueger, S. K., and S. M. Lazarus, 1999: Intercomparison of multi-day simulations of convection during TOGA COARE with several cloud-resolving and single-column models. Preprints, *23d Conf. on Hurricanes and Tropical Meteorology*, Dallas, TX, Amer. Meteor. Soc.
- Lin, Y.-L., R. D. Farley, and H. D. Orville, 1983: Bulk parameterization of the snow field in a cloud model. *J. Climate Appl. Meteor.*, **22**, 1065-1092.
- Liu, C., M. W. Moncrieff, and E. J. Zipser, 1997: Dynamical influence of microphysics in tropical squall lines: A numerical study. *Mon. Wea. Rev.*, **125**, 2193-2210.
- McCumber, M., W.-K. Tao, J. Simpson, R. Penc, and S.-T. Soong, 1991: Comparison of ice-phase microphysical parameterization schemes using numerical simulations of tropical convection. *J. Appl. Meteor.*, **30**, 985-1004.
- Moncrieff, M. W., S. K. Krueger, D. Gregory, J.-L. Redelsperger, and W.-K. Tao, 1997: GEWEX Cloud System Study (GCSS) Working Group 4: Precipitating convective cloud systems. *Bull. Amer. Meteor. Soc.*, **78**, 831-845.
- Petch, J. C., and M. E. B. Gray, 2001: Sensitivity studies using a cloud-resolving model

- simulation of the tropical west Pacific. *Quart. J. Roy. Meteor. Soc.*, **127**, 2287-2306.
- Rutledge, S.A., and P.V. Hobbs, 1984: The mesoscale and microscale structure and organization of clouds and precipitation in mid-latitude clouds. Part XII: A diagnostic modeling study of precipitation development in narrow cold frontal rainbands. *J. Atmos. Sci.*, **41**, 2949-2972.
- Shutts, G. J. and M. E. B. Gray, 1994: A numerical modeling study of the geostrophic adjustment process following deep convection. *Quart. J. Roy. Meteor. Soc.*, **120**, 1145-1178.
- Sui, C.-H., S. Li, and K.-M. Lau, 1998: Radiative-convective processes in simulated diurnal variations of tropical oceanic convection. *J. Atmos. Sci.*, **55**, 2345-2357.
- Swann, H., 1998: Sensitivity to the representation of precipitating ice in CRM simulations of deep convection. *Atmos. Res.*, **47-48**, 415-435.
- Tao, W.-K., and J. Simpson, 1989: Modeling study of a tropical squall-type convective line. *J. Atmos. Sci.*, **46**, 177-202.
- Tao, W.-K., and J. Simpson, 1993: The Goddard Cumulus Ensemble Model. Part I: Model description. *Terrestrial, Atmospheric and Oceanic Sciences*, **4**, 19-54.
- Tao, W.-K., J. R. Scala, B. Ferrier, and J. Simpson, 1995: The effect of melting processes on the development of a tropical and a midlatitude squall line. *J. Atmos. Sci.*, **52**, 1934-1948.
- Tao, W.-K., S. Lang, J. Simpson, C.-H. Sui, B. Ferrier, and M.-D. Chou, 1996: Mechanisms of cloud-radiation interaction in the tropics and midlatitudes. *J. Atmos. Sci.*, **53**, 2624-2651.
- Tao, W.-K., J. Simpson and B. Ferrier, 1997: Cloud resolving model simulations of mesoscale convective systems, new insights and approaches to convective parameterization. *Proc. ECMWF/GCSS Workshop on New Insights and Approaches to Convective Parameterization*, Reading, United Kingdom, ECMWF, 77-112.
- Tao, W.-K., S. Lang, J. Simpson, W. S. Olson, D. Johnson, B. Ferrier, C. Kummerow and R. Adler, 2000: Vertical profiles of latent heat release and their retrieval in TOGA COARE convective systems using a cloud resolving model, SSM/I and radar data, *J. Meteor. Soc. Japan*, **78**, 333-355.
- Tao, W.-K., J. Simpson, D. Baker, S. Braun, M.-D. Chou, B. Ferrier, D. Johnson, A. Khain, S. Lang, B. Lynn, C.-L. Shie, D. Starr, C.-H. Sui, Y. Wang and P. Wetzell,

- 2003: Microphysics, radiation and surface processes in a non-hydrostatic model. *Meteorology and Atmospheric Physics*, **82**, 97-137.
- Tao, W.-K., C.-L. Shie, D. Johnson, and J. Simpson, 2004: Surface energy budget and precipitation efficiency for convective systems developed during TOGA COARE, GATE, SCSMEX and ARM: Cloud-resolving model simulations. *J. Atmos. Sci.* (in press).
- Wu, X., W. W. Grabowski, and M. W. Moncrieff, 1998: Long-term behavior of cloud systems in TOGA COARE and their interactions with radiative and surface processes. Part I: Two-dimensional modeling study. *J. Atmos. Sci.*, **55**, 2693-2714.
- Wu, X., W. D. Hall, W. W. Grabowski, M. W. Moncrieff, W. D. Collins, and J. T. Kiehl, 1999: Long-term behavior of cloud systems in TOGA COARE and their ginteractions with radiative and surface processes. Part II: Effects of ice microphysics on cloud-radiation interaction. *J. Atmos. Sci.*, **56**, 3177-3195.
- Wu, X., and M. W. Moncrieff, 2000: Evaluation of large-scale forcing during TOGA COARE for cloud-resolving models and single-column models. *J. Atmos. Sci.*, **57**, 2977-2985.
- Xu, K.-M., and D. A. Randall, 1995: Impact of interactive radiative transfer on the macroscopic behavior of cumulus ensembles. Part II: Mechanisms for cloud-radiation interactions. *J. Atmos. Sci.*, **52**, 800-817.
- Xu, K.-M., and D. A. Randall, 1996: Explicit simulation of cumulus ensembles with the GATE phase III data: Comparison with observations. *J. Atmos. Sci.*, **53**, 3710-3736.
- Xu, K.-M., and D. A. Randall, 1998: Influence of large-scale advective cooling and moistening effects on the quasi-equilibrium behavior of explicitly simulated cumulus ensembles. *J. Atmos. Sci.*, **55**, 896-909.

TABLES

- Table 1 Major parameterizations incorporated into the seven simulations of this study, divided by microphysics, surface, and radiation schemes.
- Table 2 Mean sensible and latent heat fluxes for cases involving sensitivities to surface fluxes and radiation. Units are W m^{-2} .
- Table 3 Mean CAPE for cases involving sensitivities to surface fluxes and radiation.
- Table 4 Mean total precipitation (mm), and proportion which is convective and stratiform for cases involving sensitivities to surface fluxes and radiation.
- Table 5 Temperature budgets for cases involving sensitivities to surface fluxes and radiation. Net condensation (term B) is the sum of condensation, deposition, evaporation, sublimation, freezing, and melting of cloud hydrometeors. The large-scale forcing (term C) is the imposed large-scale advective effect on temperature, and term A is the local time change (over eight days of integration) of temperature. Term D is net radiative processes, and term E is the sensible heat flux contribution. Units are W m^{-2} .

$$C_p \left\langle \frac{\partial \bar{T}}{\partial t} \right\rangle = \underbrace{\langle L_v (\bar{c} - \bar{e}) \rangle}_A + \underbrace{L_s (\bar{d} - \bar{s})}_B + \underbrace{L_f (\bar{f} - \bar{m})}_C - C_p \bar{\pi} \left\langle \bar{w} \frac{\partial \bar{\theta}}{\partial z} \right\rangle + \underbrace{\langle Q_R \rangle}_D + \underbrace{C_p \bar{H}_s}_E$$

- Table 6 Water budgets for cases involving sensitivities to surface fluxes and radiation. Net condensation (term B) is the sum of condensation, deposition, evaporation, and sublimation of cloud hydrometeors. The large-scale forcing (term C) is the imposed large-scale advective effect on water vapor, and term A is the local time change (over eight days of integration) of water vapor. Term E is the latent heat flux contribution. Units are W m^{-2} .

$$L_v \left\langle \frac{\partial \bar{q}_v}{\partial t} \right\rangle = - \underbrace{\langle L_v (\bar{c} - \bar{e}) \rangle}_B - \underbrace{L_s (\bar{d} - \bar{s})}_C - L_v \left\langle \bar{w} \frac{\partial \bar{q}_v}{\partial z} \right\rangle + \underbrace{L_v \bar{E}_O}_D$$

- Table 7 Same as Table 2, except for cases involving sensitivities to microphysical processes.
- Table 8 Same as Table 3, except for cases involving sensitivities to microphysical processes.

FIGURES

- Fig. 1 Mean simulated (a) temperature differences (K), and (b) moisture differences (g/kg) from observations, for cases involving sensitivities to surface fluxes and radiation.
- Fig. 2 Mean simulated RMS (a) temperature deviations (K), and (b) moisture deviations (g/kg) from observations, for cases involving sensitivities to surface fluxes and radiation.
- Fig. 3 Domain- and time-averaged upward and downward (a) maximum vertical velocities and (b) mean vertical velocities for cases involving sensitivities to surface fluxes and radiation. Units are in m/s.
- Fig. 4 Mean (a) cloud fraction (%), and (b) relative humidity (%) for cases involving sensitivities to surface fluxes and radiation.
- Fig. 5 Mean (a) total hydrometeor mixing ratio (g/kg), and (b) cloud mass flux ($\text{kg/m}^2/\text{s}$) for cases involving sensitivities to surface fluxes and radiation.
- Fig. 6 Domain-averaged total hydrometeor mixing ratio (g/kg) for cases involving sensitivities to surface fluxes and radiation. The contour interval is 0.04 g/kg, and the minimum contour is 0.002 g/kg.
- Fig. 7 Cross-sectional total hydrometeor mixing ratio field contours (g/kg) at 18Z 24 December 1992 for cases involving sensitivities to surface fluxes and radiation. The contour intervals are 0.01, 0.1, 0.2, 0.5, 1.0, 2.0, 5.0, and 10.0 g/kg.
- Fig. 8 Same as Fig. 1, except for cases involving sensitivities to microphysical processes.
- Fig. 9 Same as Fig. 2, except for cases involving sensitivities to microphysical processes.
- Fig. 10 Same as Fig. 3, except for cases involving sensitivities to microphysical processes.
- Fig. 11 Same as Fig. 4, except for cases involving sensitivities to microphysical processes.
- Fig. 12 Same as Fig. 5, except for cases involving sensitivities to microphysical processes.
- Fig. 13 Same as Fig. 6, except for cases involving sensitivities to microphysical processes.
- Fig. 14 Same as Fig. 7, except for cases involving sensitivities to microphysical processes.

Table 1.

Simulation	Microphysics Scheme	Surface Scheme	Radiation Scheme
C512	RH	AERO	INTER
NOICE	LIQ-WAT	AERO	INTER
2ICE	KESSLER	AERO	INTER
NOMLT	RH (NO MELT)	AERO	INTER
NOSFC	RH	NONE	INTER
TOGA	RH	TOGA	INTER
NORAD	RH	AERO	NONE

Table 2.

Simulation	Sensible Heat Flux	Latent Heat Flux
OBS	14.9	136.9
C512	23.2	160.9
NOSFC	0.0	0.0
TOGA	19.0	130.6
NORAD	24.2	154.8

Table 3.

Simulation	Mean CAPE
C512	699.9
NOSFC	212.1
TOGA	644.0
NORAD	710.5

Table 4.

Simulation	Total Precipitation (mm)	Convective (%)	Stratiform (%)
C512	160.5	53.4	46.6
NOSFC	134.0	30.7	69.3
TOGA	159.3	50.5	49.5
NORAD	163.1	53.3	46.7

Table 5.

Simulation	A	B	C	D	E
C512	-56.15	719.32	-796.28	-1.91	23.17
NOSFC	-165.97	606.45	-796.28	24.56	0.0
TOGA	-58.84	713.48	-796.28	3.11	19.01
NORAD	-42.69	730.34	-796.28	0.0	24.14

Table 6.

Simulation	A	B	C	D
C512	16.36	-579.40	434.83	161.21
NOSFC	-47.93	-482.75	434.83	0.0
TOGA	10.39	-574.86	434.83	130.82
NORAD	1.57	-588.19	434.83	154.98

Table 7.

Simulation	Sensible Heat Flux	Latent Heat Flux
OBS	14.9	136.9
C512	23.2	160.9
NOICE	21.8	156.1
2ICE	24.4	159.9
NOMLT	11.4	130.4

Table 8.

Simulation	Mean CAPE
C512	699.9
NOICE	1091.4
2ICE	617.2
NOMLT	1844.9

Table 9.

Simulation	Total Precipitation (mm)	Convective (%)	Stratiform (%)
C512	160.5	53.4	46.6
NOICE	151.6	62.5	37.5
2ICE	161.7	50.9	49.1
NOMLT	152.7	23.6	76.4

Table 10.

Simulation	A	B	C	D	E
C512	-56.15	719.32	-796.28	-1.91	23.17
NOICE	-72.80	702.82	-796.28	-0.43	21.80
2ICE	-44.35	726.31	-796.28	1.99	24.38
NOMLT	-63.65	740.74	-796.28	-18.67	11.41

Table 11.

Simulation	A	B	C	D
C512	16.36	-579.40	434.83	161.21
NOICE	15.78	-575.12	434.83	156.14
2ICE	10.49	-584.40	434.83	160.10
NOMLT	17.21	-548.55	434.83	130.84

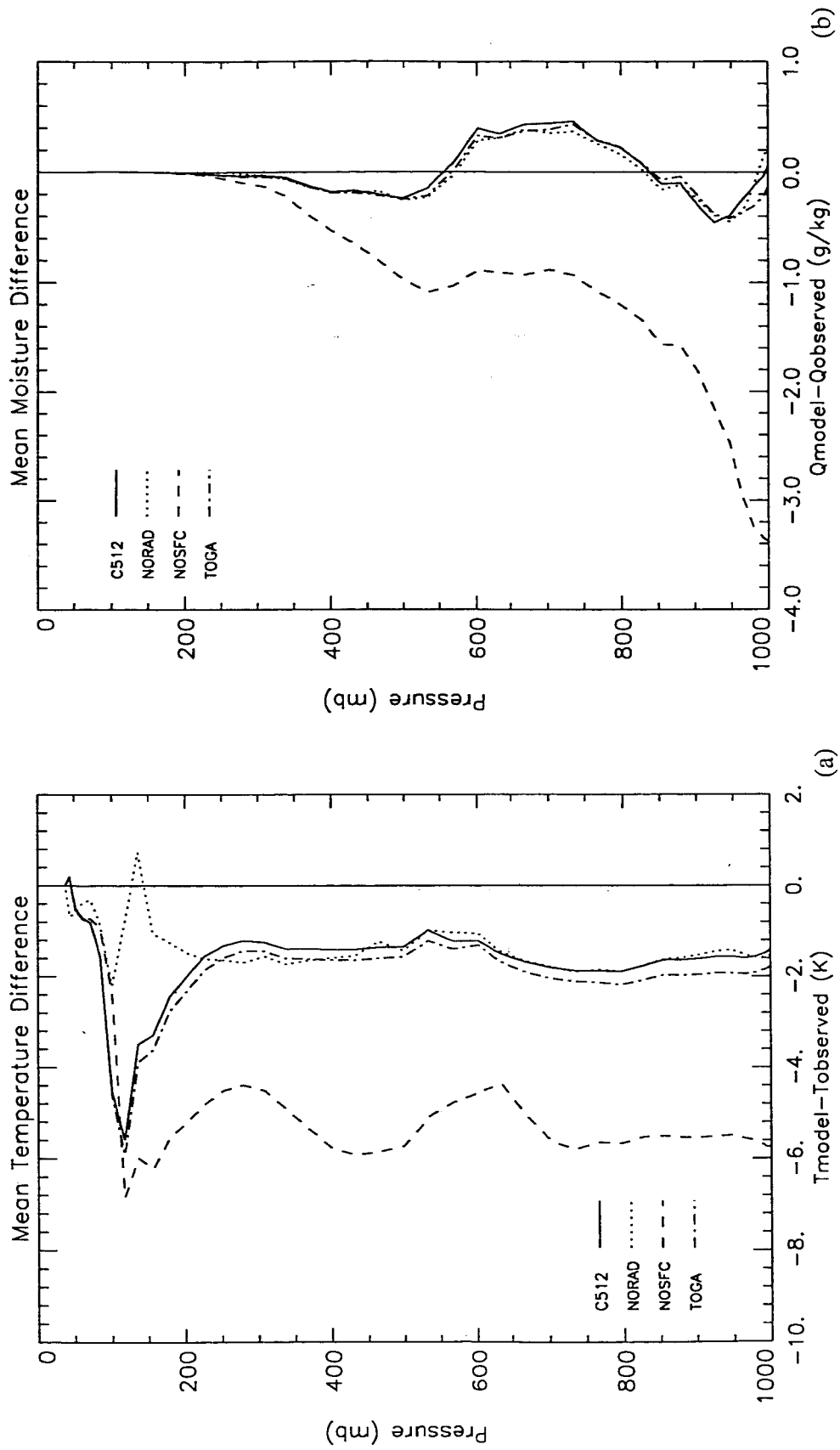


Figure 1

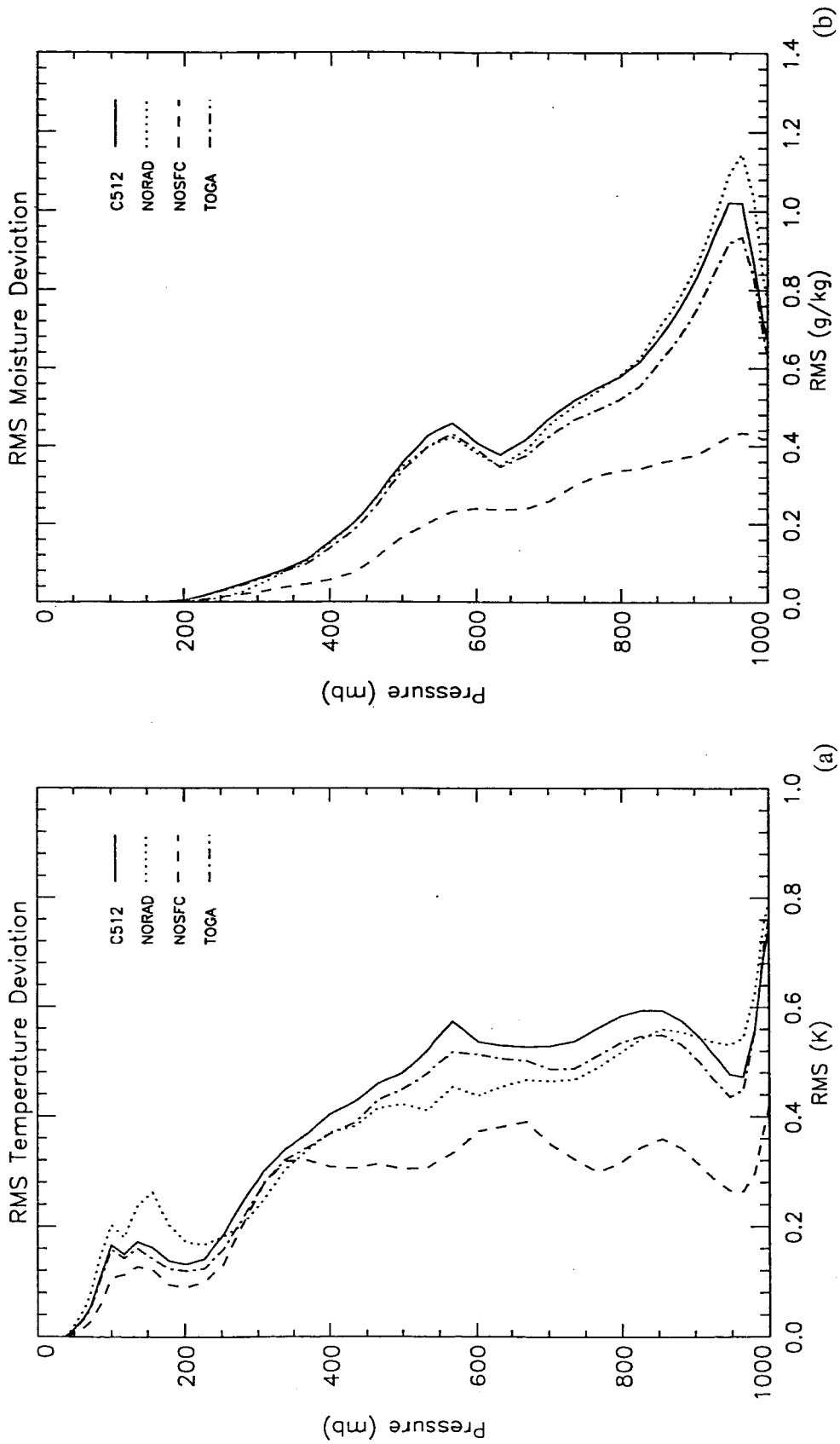


Figure 2

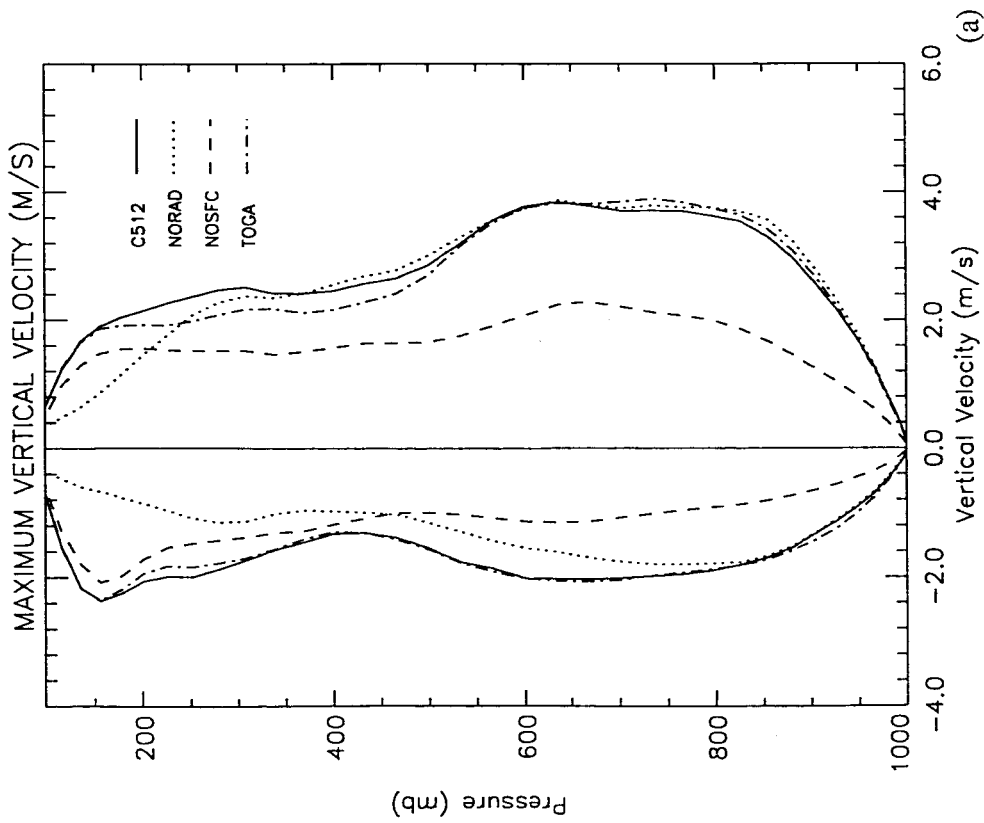
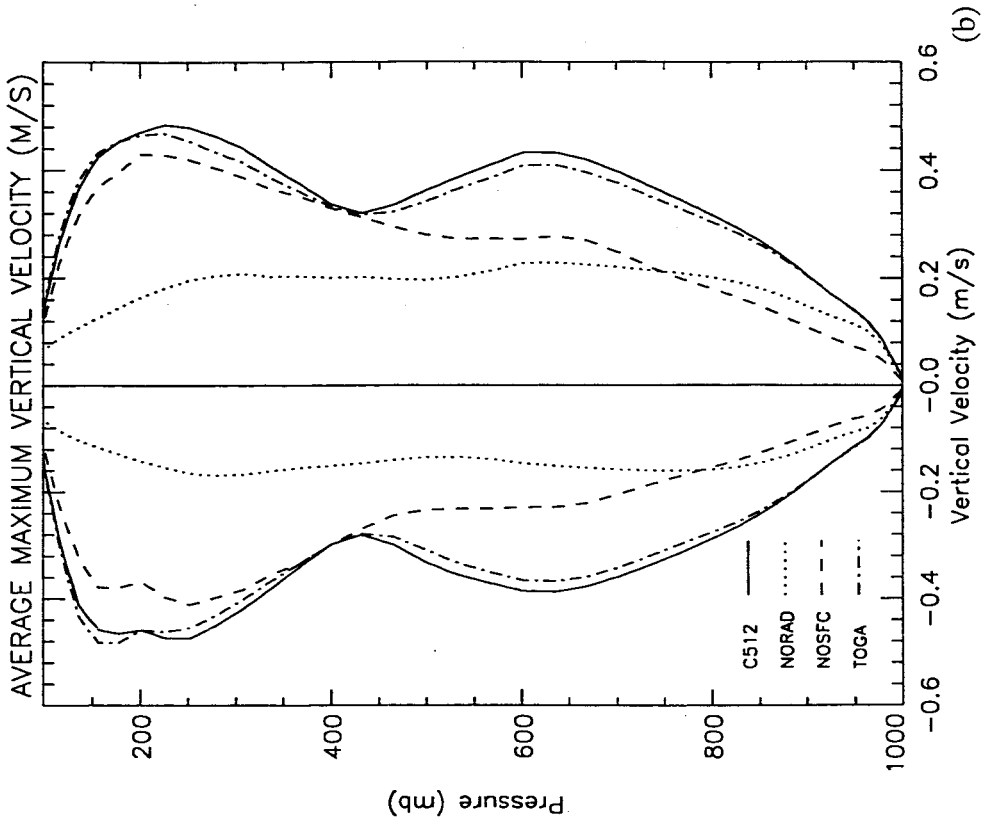


Figure 3

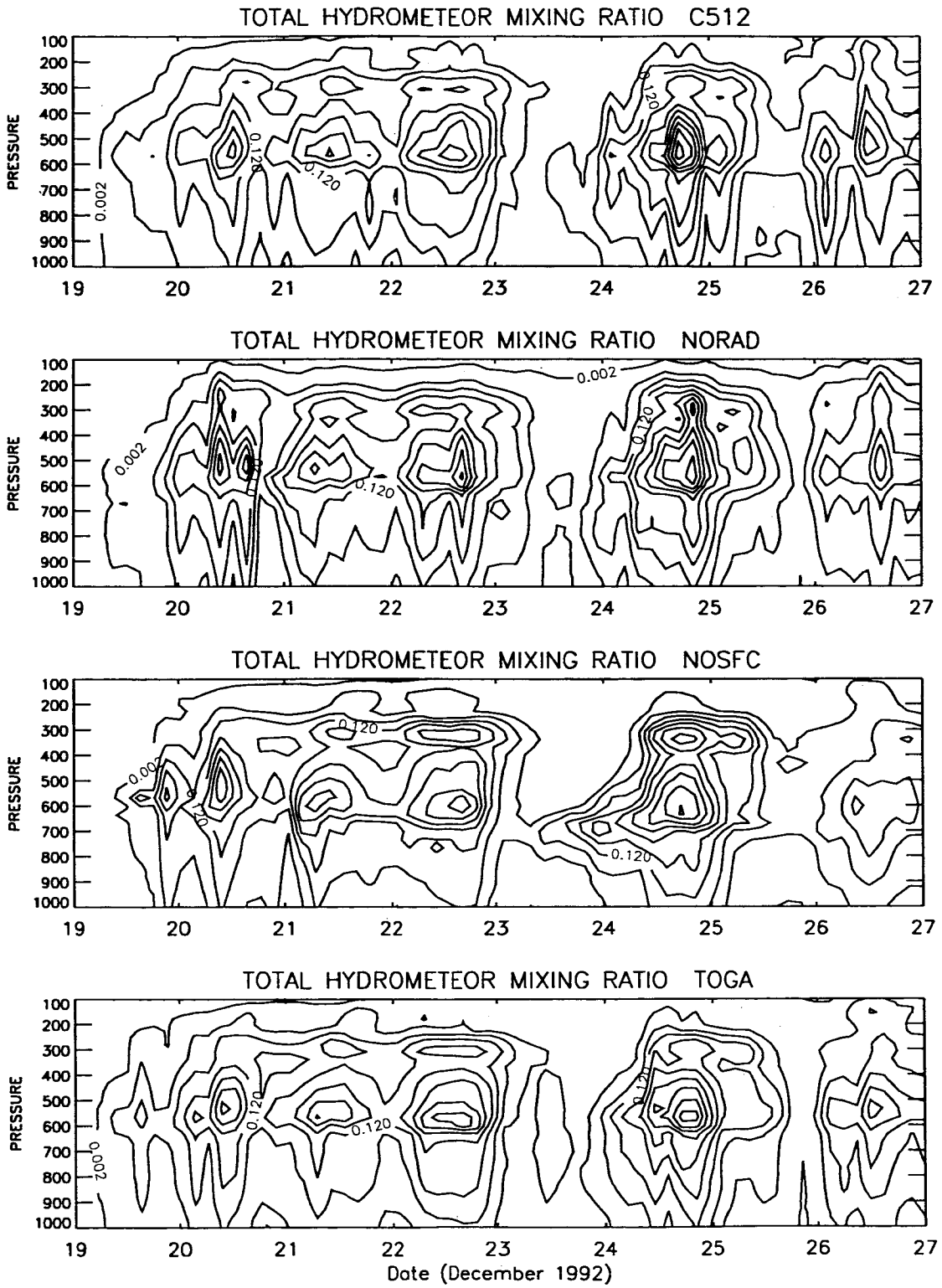


Figure 6

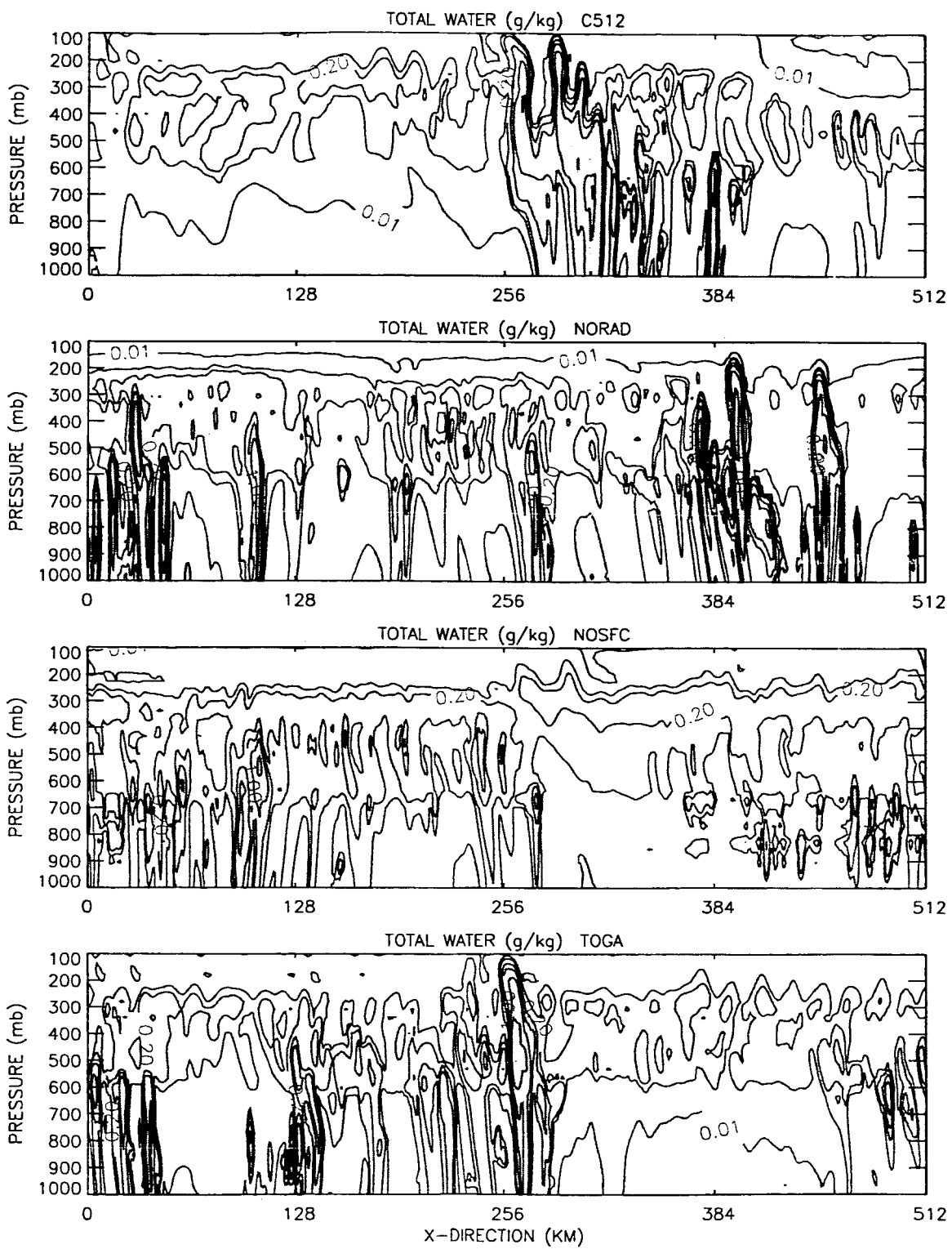


Figure 7

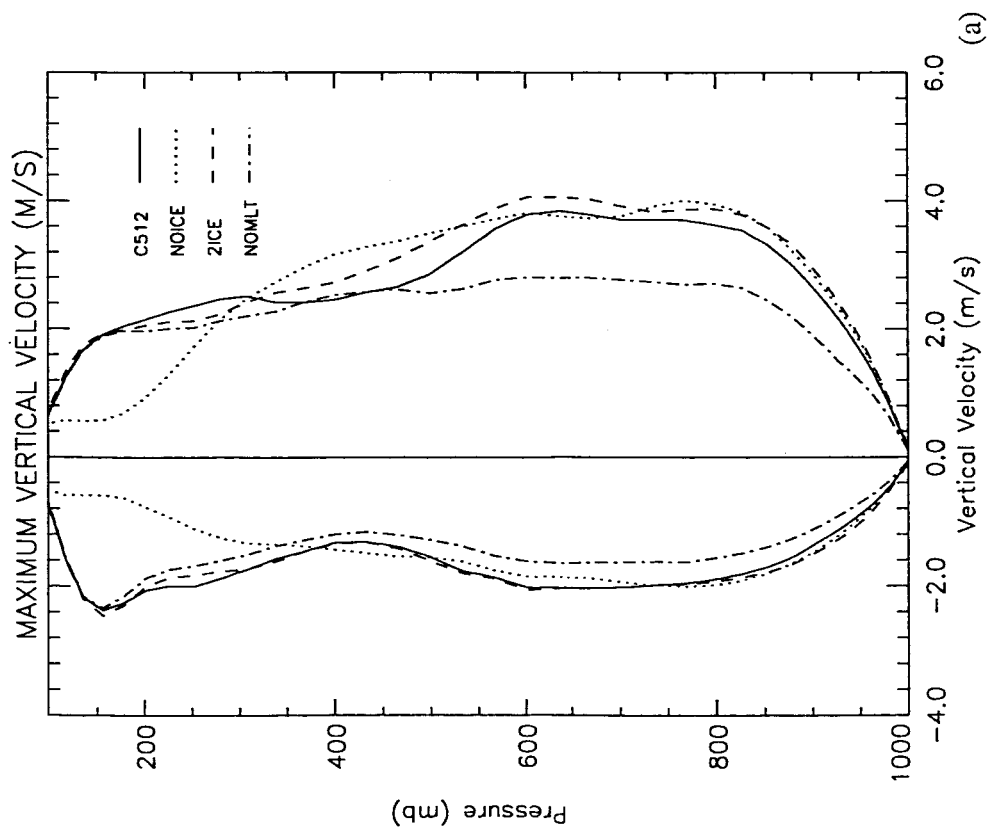
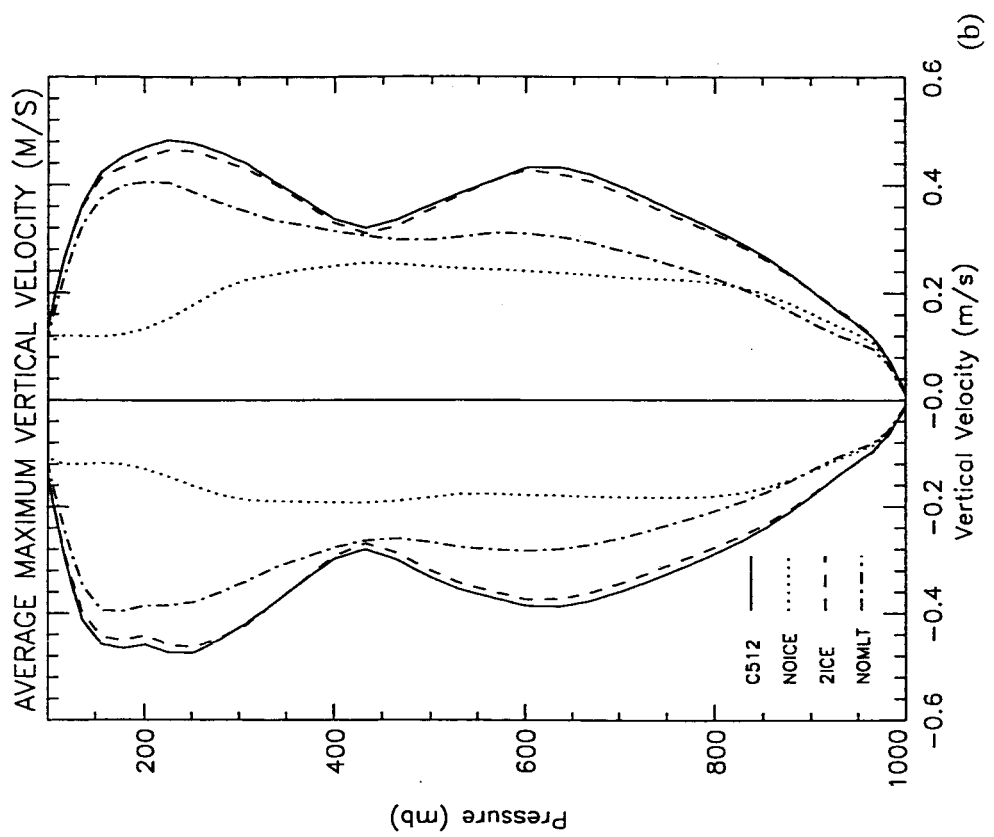


Figure 10

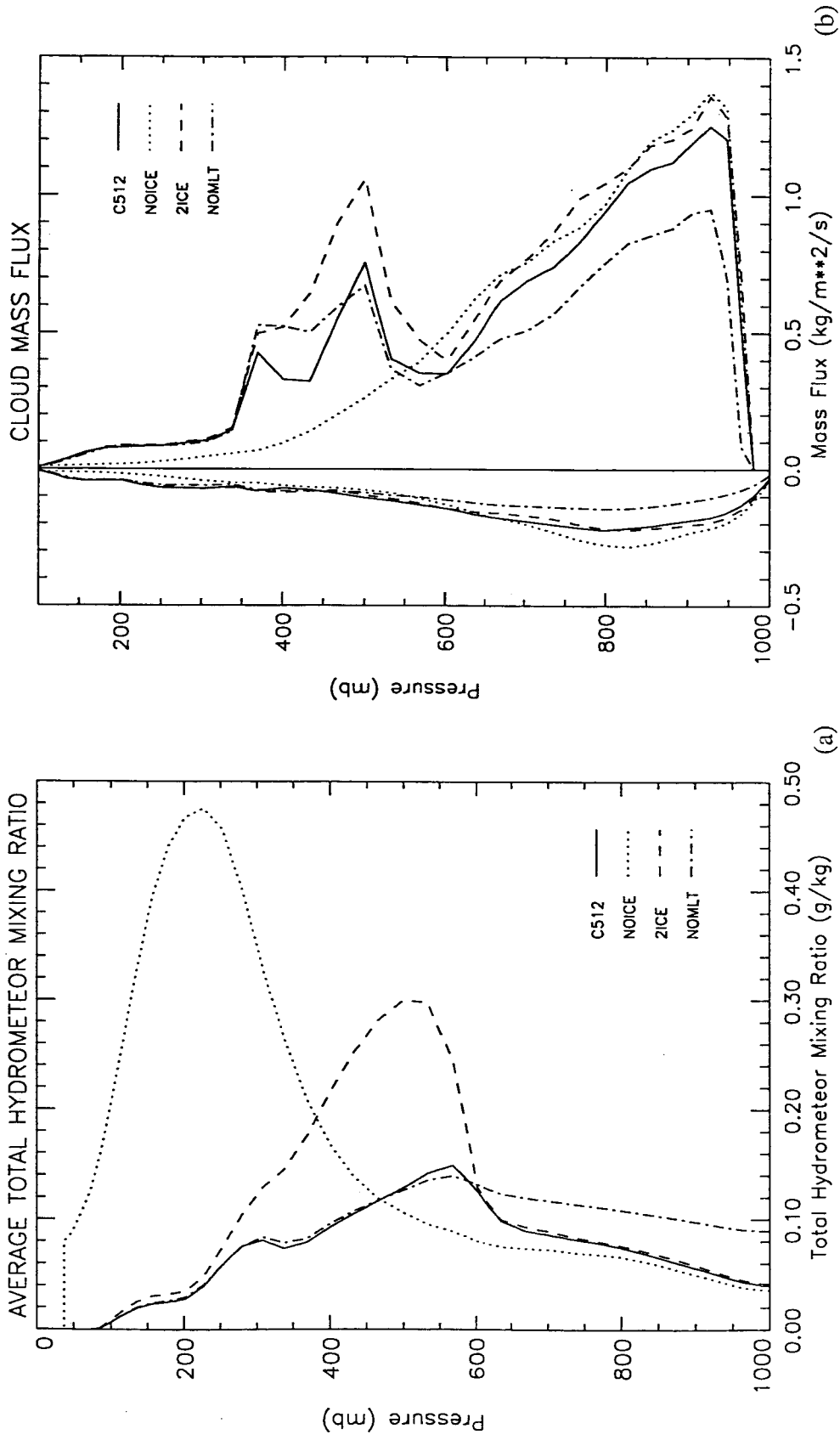


Figure 12

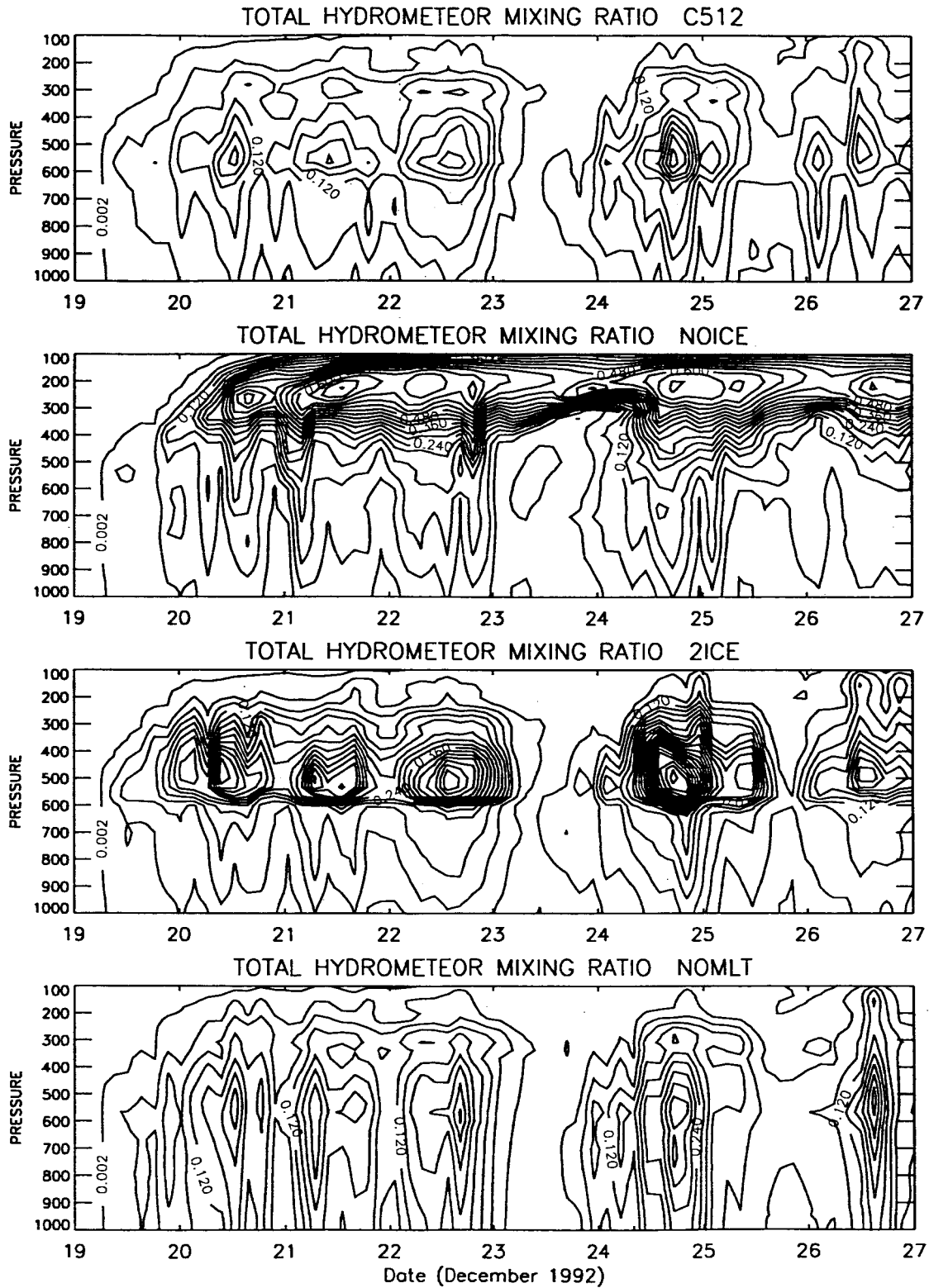


Figure 13

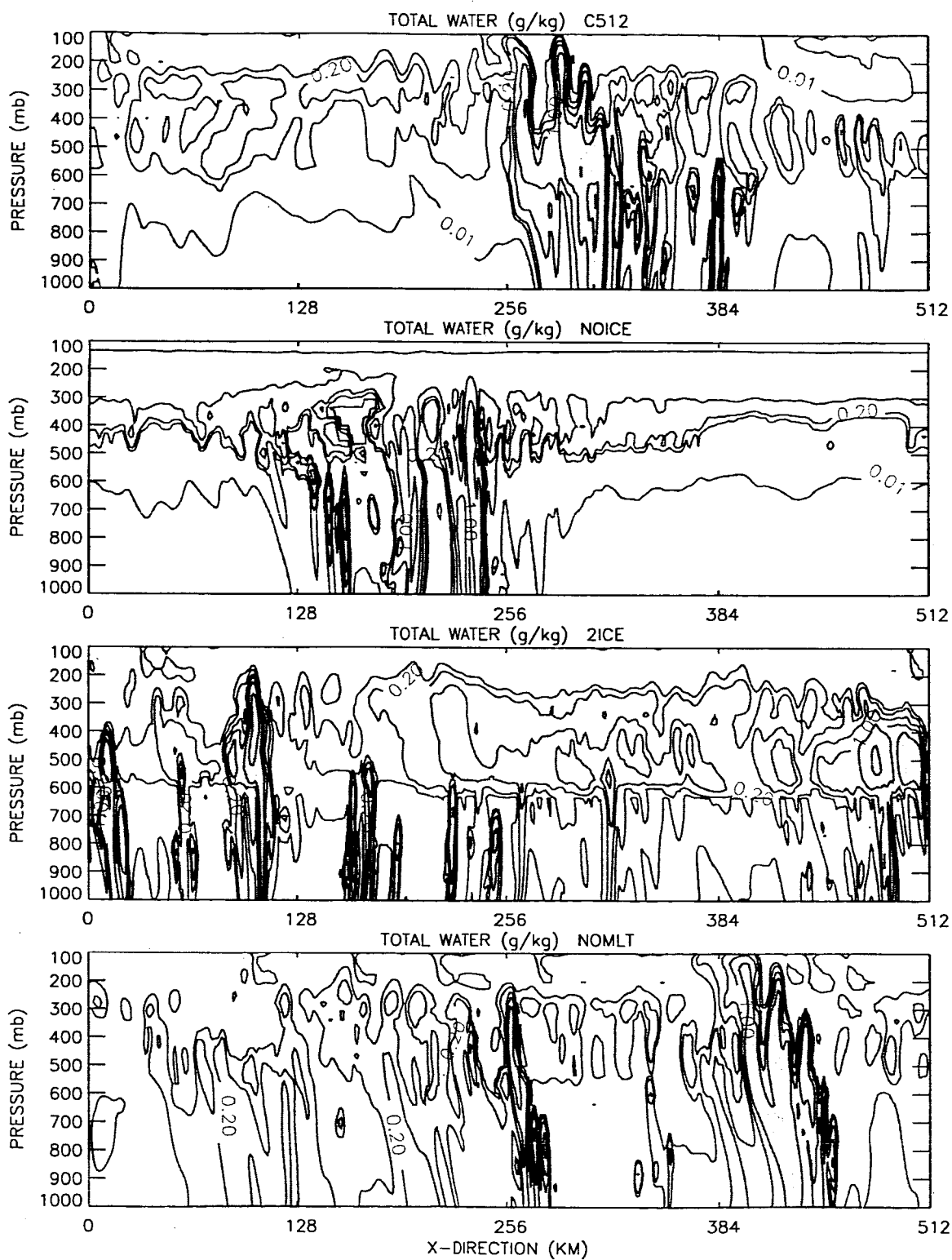


Figure 14